JOURNAL OF DEGRADED AND MINING LANDS MANAGEMENT
Volume 10, Number 2 (January 2023):4219-4232, doi:10.15243/jdmlm.2023.102.4219
ISSN: 2339-076X (p); 2502-2458 (e), www.jdmlm.ub.ac.id

Research Article

The impact of traditional gold mining on land use changes and vegetation index in Mandor Subwatershed, West Kalimantan

Lisa Astridni Putri[1], Aji Ali Akbar[1*], Romiyanto[2]

[1] Department of Environmental Engineering, Faculty of Engineering, Tanjungpura University, Jl. Profesor Dokter H. Hadari Nawawi, Pontianak, Indonesia
[2] Department of Soil Science, Faculty of Agriculture, Tanjungpura University, Jl. Profesor Dokter H. Hadari Nawawi, Pontianak, Indonesia

[*]corresponding author: aji.ali.akbar.2011@gmail.com

Article history:
Received 16 September 2022
Accepted 9 November 2022
Published 1 January 2023

Keywords:
forest
gold mining
land degradation
land use changes
remote sensing

Abstract

Traditional gold mining activities altered the environmental structure of the Mandor Subwatershed significantly. The expansion of critical land in the Mandor Subwatershed causes flooding due to the lack of water catchment areas. The purpose of this study was to identify the impact of traditional gold mining on land use change in the Mandor Subwatershed. The research was conducted with a spatial analysis approach using Landsat multitemporal images from 2002, 2013, and 2022, followed by a field survey. A comparison of the Normalized Difference Vegetation Index (NDVI) and the Enhanced Vegetation Index (EVI) methods was used to determine the changing process of vegetation density. The accuracy of vegetation index analysis indicated that the EVI method was more accurate for identifying vegetation density than the NDVI method. Land use change from 2002 to 2022 was dominated by an increase in the land area devoted to mining and oil palm plantations. The impact of this traditional gold mining has led to significant deforestation and land degradation over the past 20 years in the Mandor Subwatershed. This affects the condition of the surrounding environment as well as human health.

To cite this article: Putri, L.A., Akbar, A.A. and Romiyanto. 2023. The impact of traditional gold mining on land use changes and vegetation index in Mandor Subwatershed, West Kalimantan. Journal of Degraded and Mining Lands Management 10(2):4219-4232, doi:10.15243/jdmlm.2023.102.4219.

Introduction

Land use change is one of the important factors contributing to the degradation of environmental quality. The Mandor Subwatershed is experiencing changes in environmental conditions in line with the increase in traditional gold mining activity. Mineral mining areas themselves pose environmental, social, and food sovereignty challenges for some countries. Indigenous people and local communities are particularly vulnerable to the impacts of mining activities, especially those affecting land and water (Blanco et al., 2022). Artisanal and small-scale gold mining (ASGM) is the world's largest source of anthropogenic mercury emissions and releases (Prescott et al., 2022). Gold mining activities in the Mandor Subwatershed are carried out in water bodies, such as rivers. These open-pit mining techniques cause landform changes as well as the loss of vegetation and fauna habitats. The removal of soil above the gold deposit layer alters the topography, hydrology, and slope stability (Hidayat et al., 2015). The development of land use change is important to know to predict the pattern of land use change in the future, thus preventing and reducing the impact of gold mining (Petit et al., 2001). In addition, an overview of land use change development can be used as a reference to implement a regional policy. Information on land use and cover is necessary to track changes, set development strategies, plan for regional development, and manage natural resources (Nugroho, 2015).

Several studies on land use change modeling have been conducted in Indonesia, such as land damage and water pollution (Romiyanto et al., 2015) and identification of land conversion changes using vegetation index by utilizing satellite imagery (Yudistira et al., 2019; Husodo et al., 2021). All these studies analyzed land use and land cover, which can be monitored using satellite imagery. The spatial model produced from this research is expected to help manage and mitigate land damage due to traditional gold mining. The results of this study are expected to provide recommendations for land rehabilitation strategies in unlicensed gold mining areas in the Mandor Subwatershed. The spatial model developed by this research is intended to provide useful information for managing and mitigating land degradation caused by gold mining activities using open-pit mining techniques. Based on the problems that occur, it is necessary to conduct an analysis to identify the distribution of land changes due to mining activities and other derivative impacts in the Mandor Subwatershed. The results of this study are expected to provide recommendations for land rehabilitation strategies in unlicensed gold mining areas in the Mandor Subwatershed.

Materials and Methods

The traditional gold mining area in the Mandor Subwatershed, which is administered by Landak Regency, West Kalimantan, Indonesia, is the subject of the investigation. The research site is astronomically situated between 0°19'28.00" North and 109°20'31" East. The research area encompasses 17,000.46 hectares (Figure 1). The initial step in creating the research boundary map was to digitize the research area, the Mandor Subwatershed. Determination of research boundaries based on the topography and the flow pattern of waste generated from gold mining, which is known to be in the same network as the Mandor River.

Data preparation

Landsat satellite imagery provides a powerful tool to analyze land use change over large areas for long periods of time. Landsat imagery has a spatial resolution of 30 m, a temporal resolution of 16 days and a Sun-Synchronous orbit at an orbital altitude of 705 km (Cahyono et al., 2019). The downloaded images were Level-1 Precision and Terrain Corrected Product (L1TP) models, whose radiometric data was reliable and calibrated, as well as orthorectified using ground control points, so there was no need for geometric correction (USGS, 2016). Three satellite images, Landsat 7 ETM+, Landsat 8 OLI, and Landsat 9 OLI 2, were downloaded from the USGS-Earth Explorer portal to prepare the land use change map and vegetation index map of the upper Mandor Subwatershed in 2002, 2013, and 2022 (Table 1). To utilize the images, a radiometric correction was needed as an initial step. The purpose of radiometric correction is to remove atmospheric disturbances from satellite imagery. Because the digital number of picture pixels did not accurately represent the value of the actual object, corrections must be made to acquire the right digital pixel value to represent the actual object by estimating the disturbance and eliminating it from the image. Radiometric correction was performed through the Quantum GIS software's Semi-Automatic Classification option (Table 2). The menu converts Landsat data from digital numbers to reflectance values (Cahyono et al., 2019). The following formula is used to calculate reflectance using the DOS_1 method:

$$LP = L_{min} - LD01\% \quad \text{..... (1)}$$

$$\rho = [\pi * (L\lambda - Lp) * d^2]/(ESUN\lambda * \cos\theta) \quad \text{..... (2)}$$

Clustering or limiting the research area is the last activity of pre-image processing. The image delineation was performed by overlaying the vector data of the Mandor Subwatershed boundary with the corrected image data.

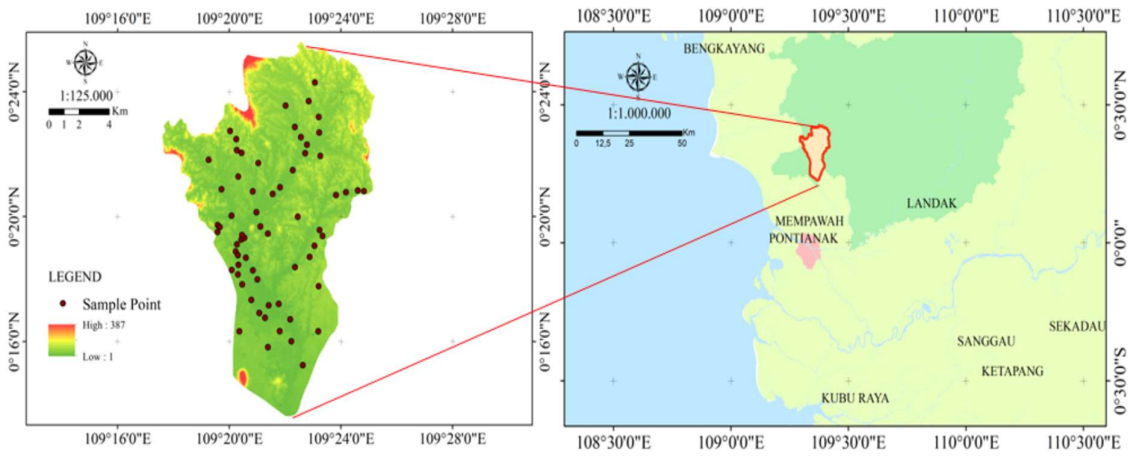

Figure 1. Map of upper Mandor Subwatershed.

Table 1. Characteristics of the Landsat images used for the study.

Sensor	Acquisition Date	Path/Row	Spatial resolution (m)	Source
Landsat 7 ETM$^+$	17 February 2002	121/ 60	30 x 30	USGS
Landsat 8 OLI	15 June 2013	121/ 60	30 x 30	USGS
Landsat 9 OLI 2	28 March 2022	121/ 60	30 x 30	USGS

Table 2. Digital number values of radiometrically corrected Landsat 7, 8, and 9 images.

Band	2002 (ETM+)		2013 (OLI)		2022 (OLI 2)	
	min	max	min	max	min	max
1	0	0.3792	0	0.6064	0	0.7673
2	0	0.4134	0	0.653	0	0.8283
3	0	0.3823	0	0.7015	0	0.8594
4	0	0.8772	0	0.763	0	0.9345
5	0	0.5261	0	0.9271	0	1

The restriction made it easier for image analysts to analyze the research area.

$$\text{Producer accuracy} = \frac{X_{ii}}{X_{i+}} \times 100\% \quad \text{.....(3)}$$

$$\text{User accuracy} = \frac{X_{ii}}{X+i} \times 100\% \quad \text{.....(4)}$$

$$\text{Overall accuracy} = \frac{\sum_{i}^{r=1} X_{ii}}{N} \times 100\% \quad \text{.....(5)}$$

$$\text{Kappa accuracy} = \frac{N \sum_{i=1}^{r} X_{ii} - \sum_{i=1}^{r} X_i + X_{+1}}{N^2 - \sum X_{i+} X_{+i}} \times 100\% \quad (6)$$

The Kappa coefficient was computed using equation 6. If the Kappa Coefficient is close to one, it reaches a perfect agreement, whereas a value close to zero means the agreement is not better (Table 3) (Rwanga and Ndambuki, 2017).

Table 3. Rating of the Kappa coefficient.

Kappa Coefficient	Strength
< 0	Poor
0 – 0.2	Slight
0.21 – 4	Fair
0.41 – 0.6	Moderate
0.61 – 0.8	Good
0.81 – 1	Very Good

Data analysis

The spatial analysis approach was used to conduct land use changes that occurred in the Mandor Subwatershed in the range of 2002 to 2022 by utilizing the Geographic Information System (GIS). Spatial modeling is an approach that provides information on land use change due to illegal mining. Land use change can be analyzed using spatial remote sensing data (Dero et al., 2021). Vegetation change studies were analyzed through remote sensing data collected from Landsat imagery, which provides multitemporal data to monitor the development and changes in vegetation density using Landsat 7, 8 and 9 imageries (Iskandar et al., 2012). The characteristics of the Landsat images used for the study is presented in Table 4. This research was conducted in four stages: pre-image processing, ground checking, image processing, and land use change analysis, along with vegetation index analysis. Land use change was analyzed using supervised classification with the maximum likelihood classification method, then ground checks were conducted to verify, and the result was presented as a land use change map. The vegetation index is a mathematical transformation that utilizes multispectral imagery and produces information about vegetation density phenomena.

Table 4. Characteristics of the Landsat images used for the study.

Land use Type	Description
Mining Area	Areas of land where the minerals are exploited using open or closed techniques
Water Body	Area of land covered with water bodies like wetlands, springs, and rivers
Palm Plantation	All appearances of cultivated perennials that belong to the plantation group
Settlement	Land used for built-up compounds and other constructed infrastructures to serve the community
Forest	Land covered by trees with forests, small trees, bushes
Rice Field	Areas cultivated for the cultivation of food crops, plantations, and horticulture
Open Land	Land without cover, whether natural, semi-natural or artificial

In this study, vegetation density was analyzed using Landsat 7, 8, and 9 image data with each recording year 2002, 2013, and 2022. The vegetation index used is a comparison of the NDVI (Normalized Difference Vegetation Index) method and the Enhanced Vegetation Index (EVI) method.

The NDVI approach calculates the green color value of vegetation using a categorization based on the value of each pixel (Yengoh et al., 2014; Siahaya et al., 2015). It could predict the occurrence and impact of natural disasters such as droughts, fires, and floods (Pettorelli et al., 2005) and predict the extent of land degradation (Prince et al., 2009). Vegetation monitoring with NDVI is suitable for environmental management given that it is a low-cost and systematic method that could identify vegetation density. NDVI remote sensing for vegetation monitoring is quite useful in assessing environmental changes (Alcaraz-Segura et al., 2009). The EVI (Enhanced Vegetation Index) transform is a refinement of the NDVI vegetation index analysis that improves the sensitivity of vegetation signals in high biomass areas. EVI improves the greenness of vegetation by combining information from the blue channel spectral band with background soil, canopy signal, and the influence of atmospheric conditions (Son et al., 2014).

Land use change analysis

Land use is defined by the purposes for which humans exploit the land. There is high variability in time and space in biophysical environments, socioeconomic activities, and cultural contexts that are associated with land use change (Lambin et al., 2003). The classification was done by the maximum likelihood classification algorithm. The image was analyzed using ArcGIS software. This method began with creating a training sample area on the composite image for each land cover. Land use changes of the study years were calculated from processed images following equations 7 and 8 (Islam et al., 2018).

Vegetation index analysis

The purpose of NDVI study is to determine the health and density of plants. In accordance with previous research, vegetation density criteria are categorized into five types. The descriptions of identified vegetation index in Mandor Subwatershed are presented in Table 5. Environmental changes lead the vegetation around the mine to lack water and nutrients, causing the leaves to appear from yellow to brown (Romiyanto et al., 2015). The NDVI algorithm is derived from the ratio between the red band and the near-infrared band. NDVI is related to the amount of photosynthetically active radiation absorbed by the plant canopy (Wang et al., 2005).

$$\text{Magnitude of change} = \text{magnitude of the new year} - \text{magnitude of the previous year} \quad \ldots\ldots(7)$$

$$\text{Percentage of land use change} = \frac{\text{magnitude of change}}{\text{base year}} \times 100\% \quad \ldots\ldots(8)$$

Table 5. Descriptions of identified vegetation index in Mandor Subwatershed.

Vegetation Index	Description
Non-Vegetation	mining area, bare land and build-up area (residential, transportation, social complexes, and services).
Low-Density Vegetation	low dense growth plants, and underbrush.
Quite-Low Density Vegetation	quite low-dense growth plants and underbrush.
Medium Density Vegetation	medium-dense growth of trees, plants, and underbrush
High-Density Vegetation	dense growth of trees and plants.

The NDVI is the most often used vegetation index. The normalized difference between the red and near-infrared bands was used to determine NDVI per unit pixel (equation 9).

$$\text{NDVI} = \frac{\text{NIR}-\text{RED}}{\text{NIR}+\text{R}} \quad \ldots\ldots(9)$$

The Enhanced Vegetation Index (EVI) analysis is the outcome of a mathematical combination of the blue, red, and near-infrared (NIR) bands. The EVI algorithm is also intended to be more sensitive to photos with highly green or dense areas (Sudiana and Diasmara, 2008). The EVI vegetation index was created to reduce the impact of canopy backdrop and atmospheric fluctuations more effectively than the NDVI (Andana, 2015).

$$\text{EVI} = \text{G}\ \frac{\text{NIR}-\text{RED}}{(\text{L}+\text{NIR}+\ \text{C}_1\ \text{Red}+\ \text{C}_2\text{Blue})} \quad \ldots\ldots(10)$$

Results

Accuracy Assessment

Accuracy assessment of land use changes

The number of accurate test point locations taken is 65, which is divided by class and then matched with field observations. The accuracy evaluation of the 2022 Landsat 9 image using the 7-5-4 band combination resulted in an overall accuracy of 94% and a Kappa accuracy of 92%. This states that of all the pixels used, 92% of the pixels were correctly classified. For Landsat 8 in 2013, using the 7-5-4 band combination resulted in an overall accuracy of 85% and Kappa accuracy of 80%. For Landsat 7 in 2002, using the 5-4-3 band combination resulted in an overall accuracy of 86% and Kappa accuracy of 80%. The findings of the land use change accuracy calculations in 2002, 2013, and 2022 are presented in Table 6.

Table 6. Accuracy of land use change analysis in 2002, 2013, and 2022.

Year	Accuracy of			
	Average Producer	Average User	Overall	Kappa
2002	79%	75%	86%	80%
2013	91%	86%	85%	80%
2022	94%	93%	94%	92%

Accuracy assessment of vegetation index

Direct observation of the field aimed to adjust the interpretation results of NDVI and EVI classifications with the real conditions of vegetation density in the field. In 2002, each NDVI and EVI approach yielded accuracy scores of 83% and 85%; in 2013, these values increased to 86% and 85%; and in 2022, they decreased to 72% and 80%. According to the image categorization, 47 out of 65 field test points with the NDVI method in 2022 will be right. In contrast, it is known that 52 of the 65 field test points used in the EVI approach in 2022 are correct. The findings of the vegetation index accuracy calculations in 200, 2013, and 2022 are presented in Table 7.

Table 7. Accuracy of vegetation index analysis in 2002, 2013, and 2022.

Normalized Difference Vegetation Index (NDVI)	
Year	**Overall Accuracy**
2002	83%
2013	86%
2022	72%
Enhanced Vegetation Index (EVI)	
Year	**Overall Accuracy**
2002	85%
2013	85%
2022	80%

Land use changes in the upper Mandor Subwatershed

The combination of land use in 2002 with the largest decrease was dominated by the forest of 11,180.52 hectares, which in 2013 decreased to 5,321.97 hectares, and then in 2022 continued to decrease to 2,953.71 hectares (Figures 2, 3 and 4). Furthermore, the decrease in land use in the water body classification was noted in 2002 as 917.73 hectares and increased to 1,521.09 hectares in 2013 and then decreased to 869.31 hectares. The decrease also happened in the settlement area, which in 2002 amounted to 1,440.63 hectares and fell to 1,280.18 hectares in 2022. Meanwhile, within a period of 20 years, the type of land that has the highest increased area was oil palm plantation land, which in 2002 was 1,691.01 hectares and has increased to 6,271.46 hectares in 2013 and continues to increase in 2022 to an area of 6,862.86 hectares. Thus, followed by an increase in the mining classification area, which originated in 2002 was 476.01 hectares, the increase in land use classes was followed by the rice fields and open land classes. This means that within a period of 20 years, from 2002 to 2022, there was a conversion of forest land into oil palm plantations and mining. It is expected that the Mandor Subwatershed's high rate of land use conversion from forest category to mining will have a detrimental influence, specifically the occurrence of river erosion and sedimentation, which can result in flooding resulting from the loss of water catchment areas.

Results presented in Table 8 show that there was a high expansion of palm plantations and mining areas at the expense of other land uses. Data presented in Tables 8 and 9 show the detailed land conversion on the upper Mandor Subwatershed from 2002 to 2022, with bold-red numbers indicating reduction and bold-black numbers indicating expansion.

Vegetation density in the upper Mandor Subwatershed

The findings of NDVI transformation density values in Mandor Subwatershed are non-vegetation, low-density vegetation, quite-low-density vegetation, medium-density vegetation, and high-density vegetation (Table 10). The NDVI scale ranges from -1.0 to 1.0.

Table 8. Area of land use on upper Mandor Subwatershed during 2002-2022.

No	Type of land use	Area					
		2002 (ETM$^+$)		2013 (OLI)		2022 (OLI 2)	
		ha	%	ha	%	ha	%
1	Mining Area	476.01	2.80	1,296.58	7.63	**2,200.77**	12.95
2	Water Body	917.73	5.40	1,521.09	8.95	**869,31**	5.11
3	Palm Plantation	1,691.01	9.95	6,271.46	36.89	**6,862.86**	40.37
4	Settlement	1,440.63	8.47	1,238.36	7.28	**1,280.18**	6.35
5	Forest	**11,180.52**	65.77	5,321.97	31.30	**2,953.71**	17.37
6	Rice Field	518.94	3.05	528.49	3.11	**894.40**	6.44
7	Open Land	775.62	4.56	822.51	4.84	**1,939.23**	11.41
	Total	17,000.46	100	17,000.46	100	17,000.46	100

Note: bold-red numbers represent a decrease; bold-black numbers represent an increase.

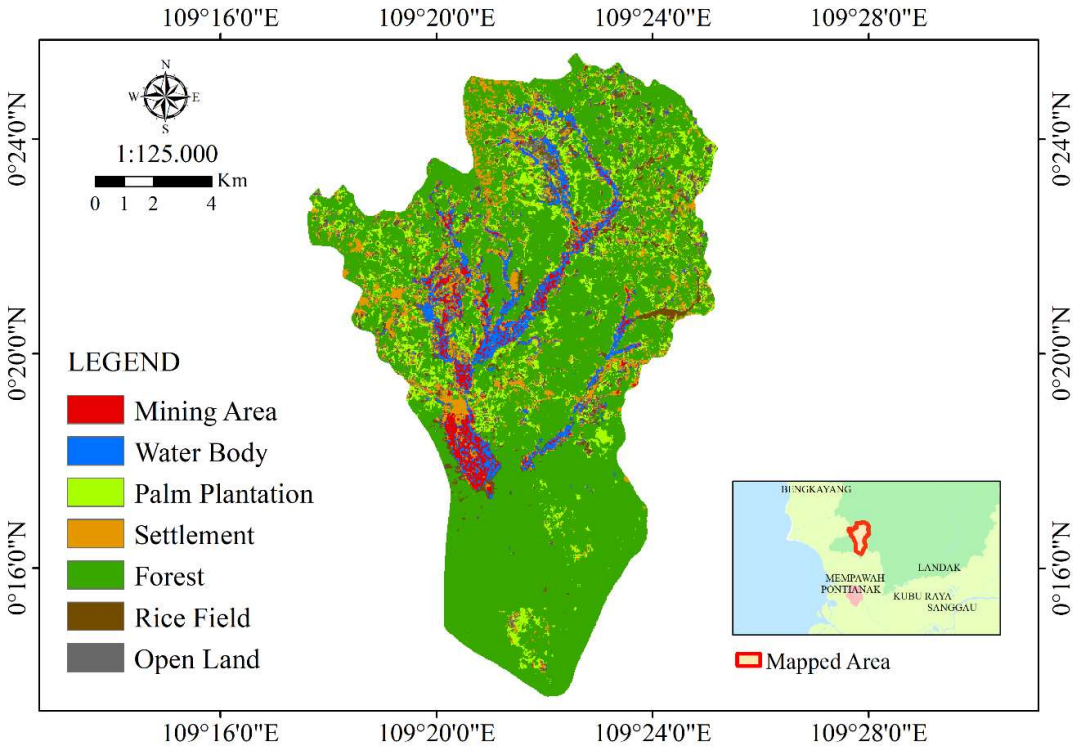

Figure 2. Mandor Subwatershed land use in 2002.

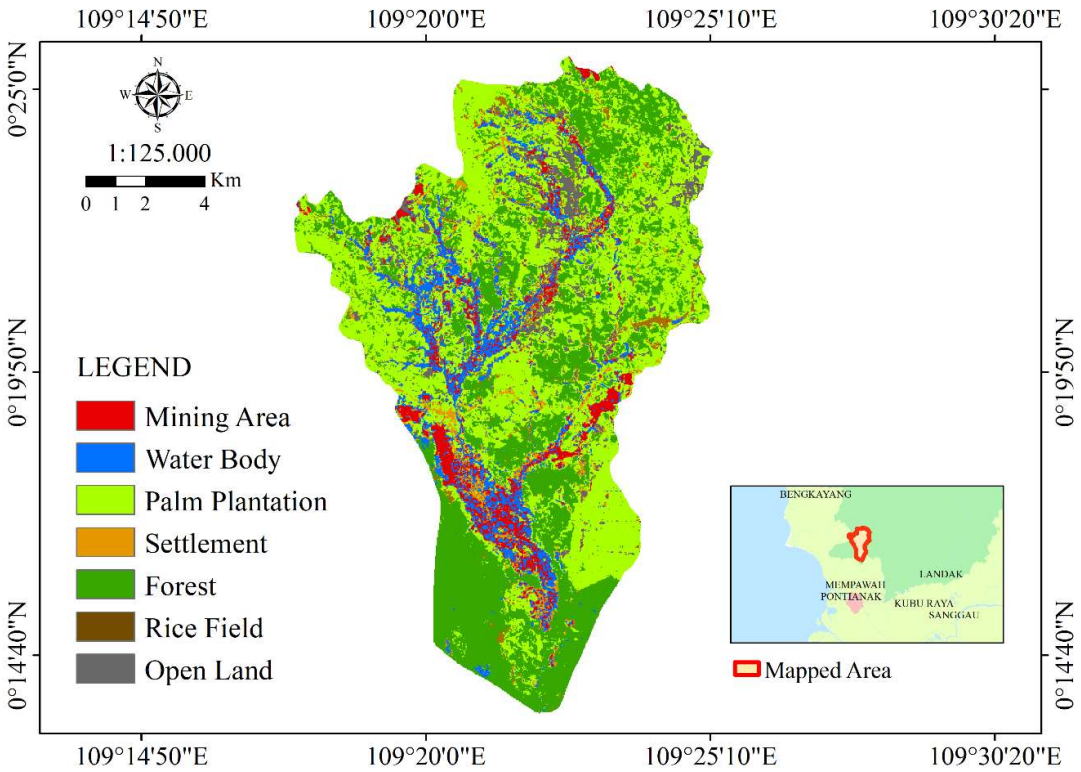

Figure 3. Mandor Subwatershed land use in 2013.

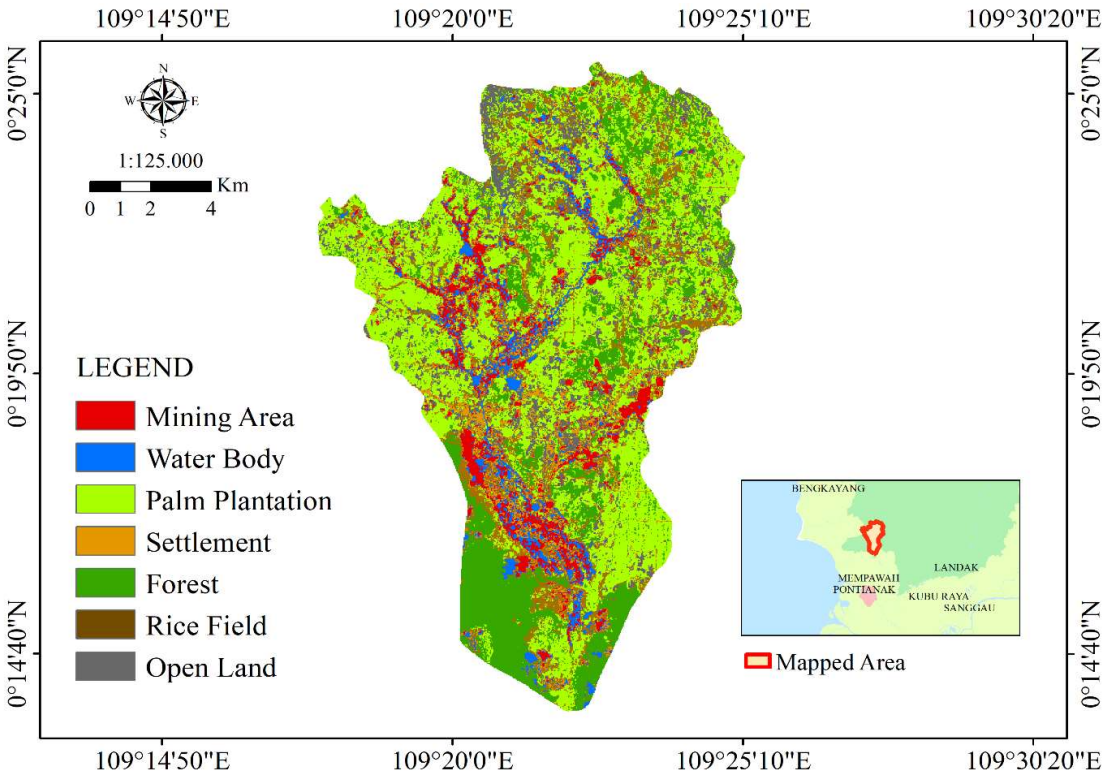

Figure 4. Mandor Subwatershed land use in 2022.

Table 9. The magnitude of land use change during 2002-2022.

No	Type of land use	Area (ha)		
		2002 - 2013	2013 - 2022	2002 - 2022
1	Mining Area	820.57	904.19	1,724.76
2	Water Body	603.36	**651.78**	**48.42**
3	Palm Plantation	4,580.45	591.4	5,171.85
4	Settlement	**202.27**	41.82	**160.45**
5	Forest	**5,858.55**	**2,368.26**	**8,226.81**
6	Rice Field	9.55	365.91	375.46
7	Open Land	46.89	1,116.72	1,163.61

Note: bold-red numbers represent a decrease; bold-black numbers represent an increase.

Table 10. Area of the index vegetation using NDVI on upper Mandor Subwatershed during 2002-2022.

No	Type of index vegetation using NDVI	Area					
		2002 (ETM^+)		2013 (OLI)		2022 (OLI 2)	
		ha	%	ha	%	ha	%
1	Non-Vegetation	689.14	4.05	768.49	4.52	771.92	4.54
2	Low-Density Vegetation	702.44	4.13	907.12	5.34	1,017.33	5.98
3	Quite Low-Density Vegetation	1,183.61	6.96	975.32	5.74	1,536.44	9.04
4	Medium Density Vegetation	4,537.48	26.69	4,198.78	24.70	2,880.09	16.94
5	High-Density Vegetation	9,887.79	58.16	10,150.75	59.71	10,794.68	63.50
	Total	17,000.46	100	17,000.46	100	17,000.46	100

Based on the calculation, the area of the most prominent high-density class changes each year. The vegetation index class is high if the land surface is still primarily covered by dense vegetation, and quite a few protecting trees between canopies are touching each other, and some are not. The high-density class using the NDVI technique amounted to 9,887.79 hectares in 2002, 10,150.75 hectares in 2013, and 10,794.68 hectares of the total area in 2022.

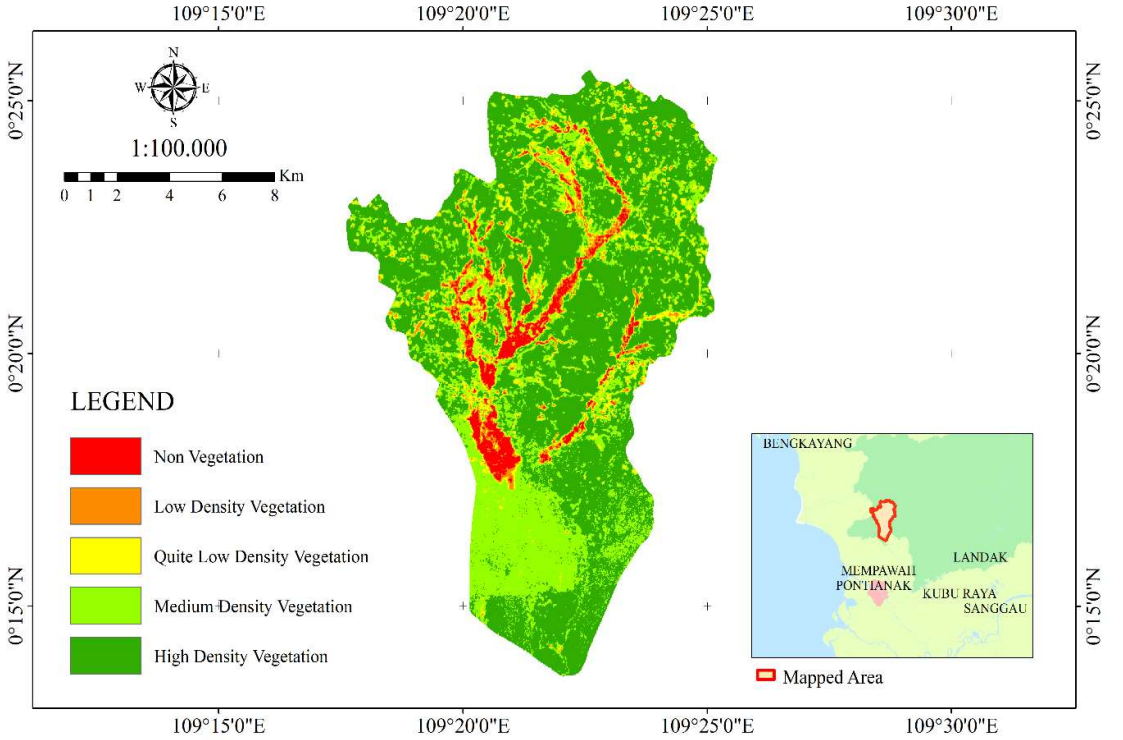

Figure 5. Index vegetation using Landsat 7 ETM^{+} of 2002 (NDVI method).

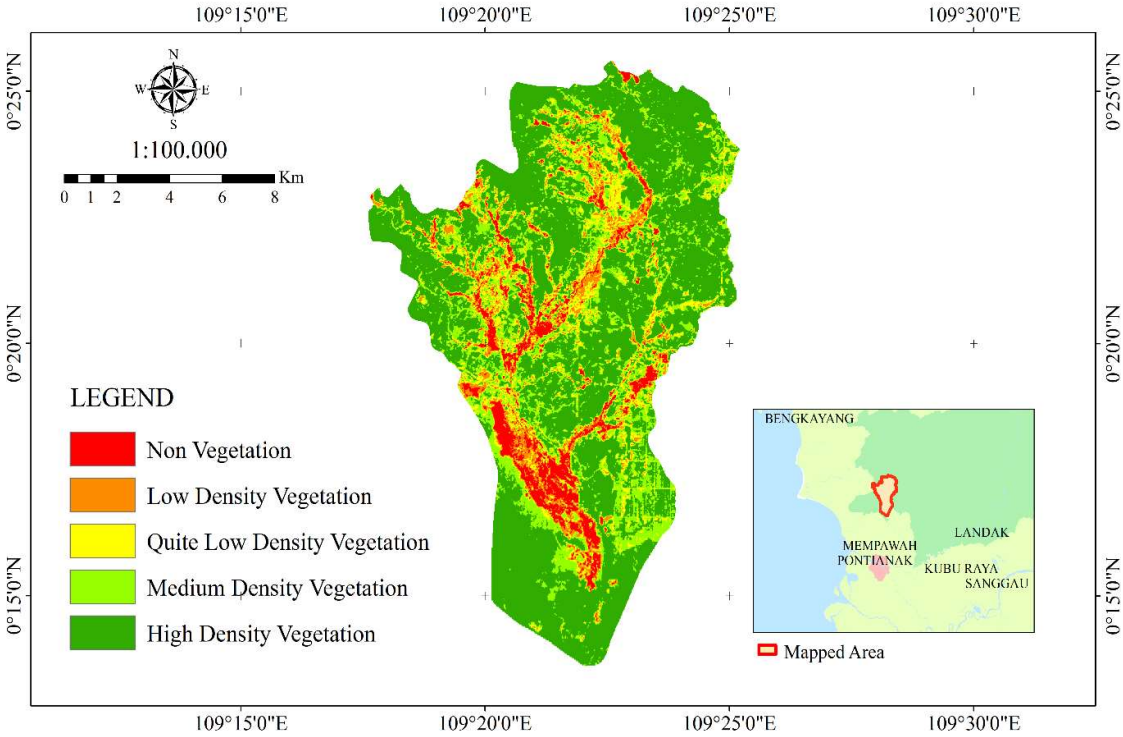

Figure 6. Index vegetation using Landsat 8 OLI of 2013 (NDVI method).

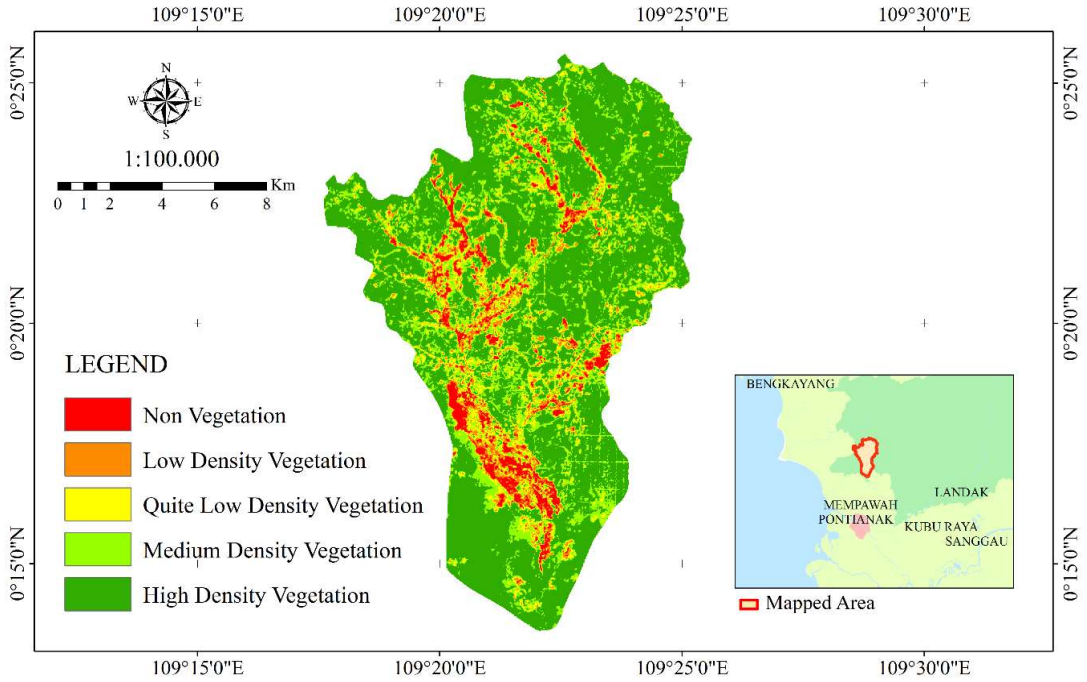

Figure 7. Index vegetation using Landsat 9 OLI 2 of 2022 (NDVI method).

The calculation results show that there was a dominant change in area with each of the first orders in the medium density, high density, moderately low density, low density, low density, and non-vegetation classes. Changes in high-density areas utilizing the EVI approach grew from 10,007.087 hectares to 10,298.32 hectares and then to 10,376.96 hectares in 2002, 2013, and 2022, respectively. Areas of low vegetation are shown in red; areas of low-density vegetation are shown in orange; areas of moderately low density are marked in yellow; areas of medium density are marked in light green; and areas marked in dark green are high-density areas (Figures 5, 6 and 7). Looking at the image, areas with a low level of plant density can be identified by light color. This is because the reflection of the vegetation crown is minimal; therefore, what appears in the image is lighter in color. Areas with a high plant density are portrayed in a darker green color due to the reflection of the thick vegetation canopy. The greenness level of vegetation can be assessed by analyzing the highest value of NDVI and EVI categorization. The greatest NDVI value for the 2002 Landsat 7 image was 0.786. In 2013, the Landsat 8 image recorded a maximum NDVI value of 0.892, while in 2022, the Landsat 9 image produced a maximum value of 0.906. The data demonstrate that the maximum NDVI value increases from 2002 to 2022.

Table 11. Area of the index vegetation using NDVI on upper Mandor Subwatershed during 2002-2022.

No	Type of index vegetation using EVI	Area					
		2002 (ETM+)		2013 (OLI)		2022 (OLI 2)	
		ha	%	ha	%	ha	%
1	Non-Vegetation	722.01	4.25	983.99	5.79	1,370.49	8.06
2	Low-Density Vegetation	716.83	4.22	913.89	5.38	1,004.17	5.91
3	Quite Low-Density Vegetation	1,560.42	9.18	623.30	3.67	627.23	3.69
4	Medium-Density Vegetation	3,994.12	23.49	4,180.96	24.59	3,621.61	21.30
5	High-Density Vegetation	10,007.08	58.86	10,298.32	60.58	10,376.96	61.04
	Total	17,000.46	100	17,000.46	100	17,000.46	100

There was a dominant change in area with the EVI method from the high-density class, which continued to increase from 10,007.08 hectares in 2002 to 10,298.32 hectares in 2013 and continued to increase to 10,376.96 hectares in 2022 (Table 11, Figures 8, 9 and 10). This was also followed by the non-vegetation and low-density classes. Meanwhile, the quite low-density class experienced the largest decrease from 1,560.42 hectares in 2002 to 623.30 hectares in 2013, then in 2022 to 627.23 hectares.

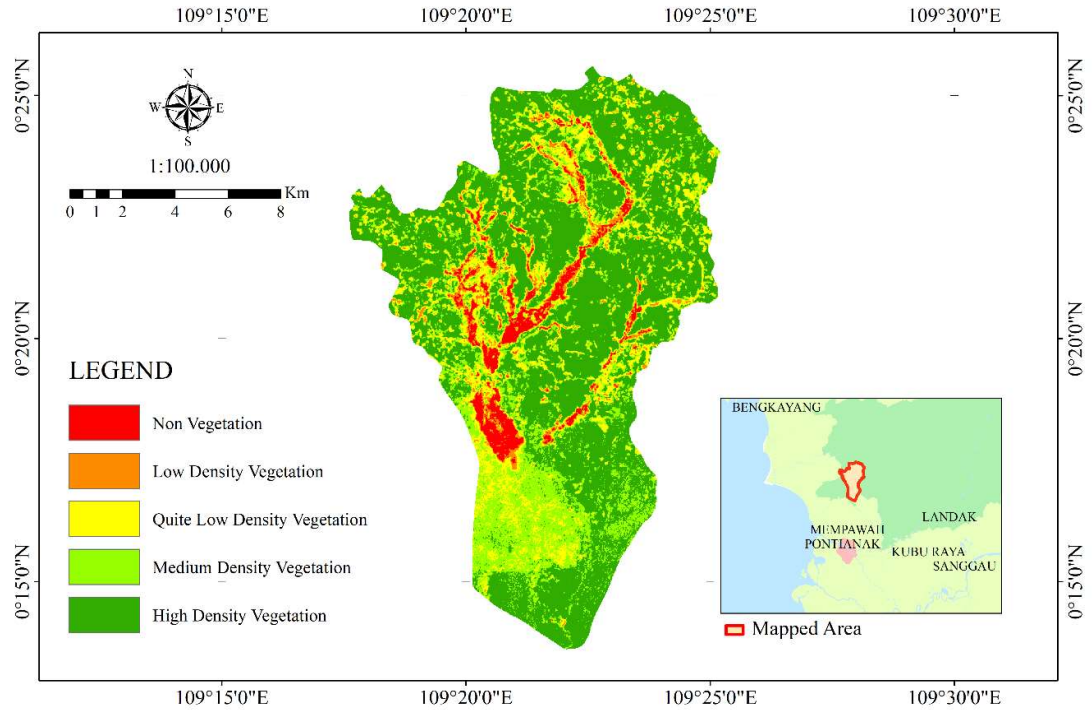

Figure 8. Index vegetation using Landsat 7 ETM^{+} of 2002 (EVI method).

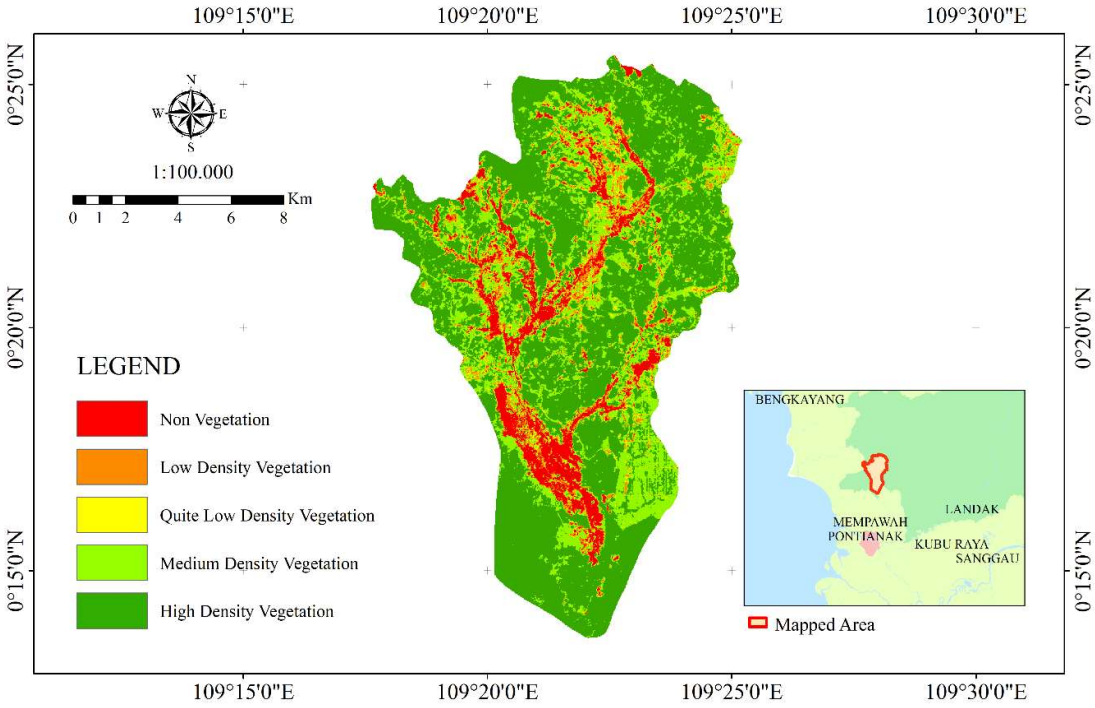

Figure 9. Index vegetation using Landsat 8 OLI of 2013 (EVI method).

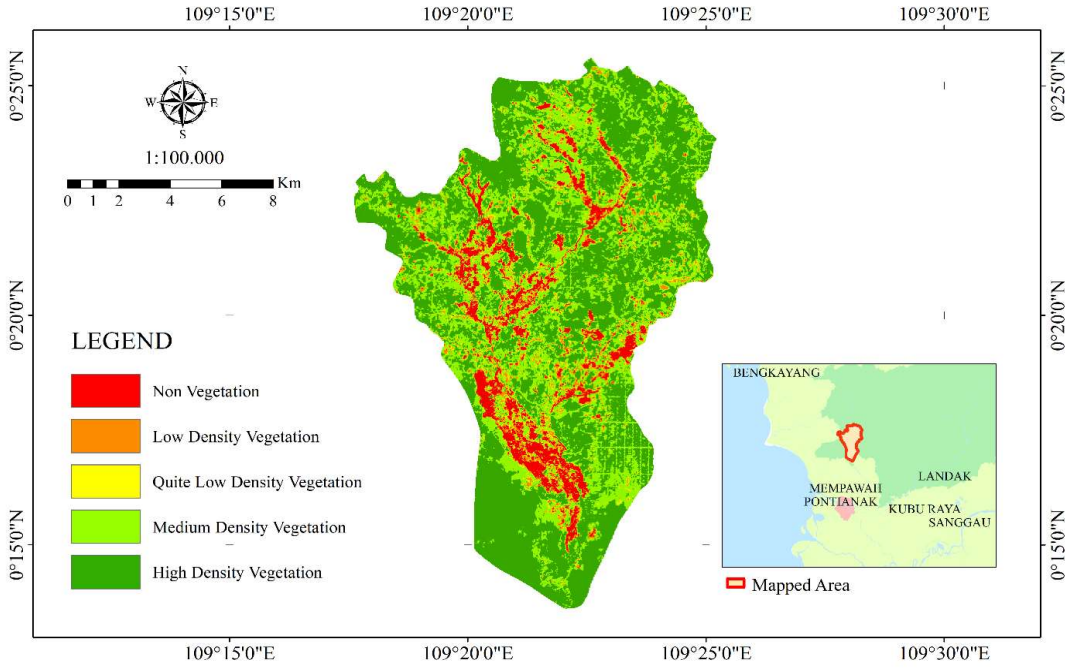

Figure 10. Index vegetation using Landsat 9 OLI 2 of 2022 (EVI method).

The EVI index value is high because the vegetation index is proportional to photosynthetic activity; the EVI value increases as photosynthetic activity increases, and the biomass in the study area is greener (Carvalho et al., 2008).

Discussion

The expansion of mining areas occurs along with the degradation of forested land. This problem is widespread around the world in regions where mining operations are conducted on forest land. The effects of traditional gold mining are undoubtedly not limited to the mine site but also have a greater impact on areas outside of the mining area, such as villages, rice fields, and oil palm plantations (Seki et al., 2022). According to Table 7 about land use changes, the impact of gold mining led to an increase in critical land area of 1,163 ha and 8,226 ha of deforestation between 2002 and 2022. However, it is also possible that this indication is a result of the mining activity's indirect appeal, which led to the formation of settlements with a range of activities, including oil palm plantations, as well as an increase in the area of about 5,171 ha over a 20-year period.

The degradation of forest areas will also have an impact on climate change (Kahhat et al., 2019; Islam et al., 2020). At the study site, it is believed that the loss of forest land is a direct result of gold mining, which has also increased the area devoted to oil palm plantations; this loss will increase greenhouse gases in the atmosphere. Ulrich et al. (2022) stated that global greenhouse gas (GHG) emissions from gold mining exceed 100 Mt of CO_2-e per year. The environmental cost to gold miners is estimated to be between US$50 t^{-1} CO_2-e and US$100 t^{-1} CO_2-e. The impact of carbon price varies widely between countries; with a gold price of US$100 t^{-1} CO_2-e, the average production cost is US$13 per ounce in Finland and up to US$275 per ounce in South Africa.

Activities related to artisanal and small-scale gold mining are a significant global source of mercury (Hg) emissions into the atmosphere. Mercury was used in the Mandor Subwatershed's traditional gold mining process to separate gold from other materials, which produced sand and gold as byproducts. The downstream flow and tidal processes can also spread mercury contamination. Flooding-related infiltration may accelerate the movement of contaminants into the soil (Liu et al., 2021). Mercury contamination may adhere to sediments and result in water pollution. Elevated levels of dissolved total mercury and methylmercury (MeHg) in the water and sediment are signs of local contamination. Artisanal gold mining contributed 12% of atmospheric Hg deposition, 10% of plankton methylmercury concentrations, and 0.63% of total soil Hg concentrations (Pang et al., 2022). Besides that, carnivores had larger bioaccumulation factors in relation to dissolved MeHg than omnivores, and they varied by area, which suggests that factors other than MeHg concentration alone were influencing absorption and trophic transmission (Mason et al., 2019). Furthermore, mercury pollution in shrimp in the Mandor River is almost evenly distributed, which indicates that the pattern of mercury distribution in sediments in the Mandor River has increased levels downstream (Triana et al., 2013).

Based on the Environmental Service of Landak Regency in 2021 on examination of dissolved residues, suspended residues, pH, BOD (biological oxygen demand), COD (chemical oxygen demand), DO (dissolved oxygen), and iron (Fe), then compared with the water quality standards of class II according to Government Regulation Number 22 of 2021, the Mandor River has exceeded the threshold. This means that Mandor river waters are not good for the life and reproduction of aquatic organisms. Water pollution increases the risk of developing skin conditions or other illnesses (Mailendra and Buchori, 2019). Mercury levels that exceed the threshold show the influence on the health of people who live long enough in the gold mining area. Additionally, it is suspected that mercury poisoning contributes to 1,430 annual deaths worldwide and a 5.8-point drop in intellect. When compared to health-related effects, these negative effects are estimated to be worth $154 billion, which is 1.5 times the local impact (Pang et al., 2022). Clinical malaria and dengue fever cases, which are transmitted through the bites of *Aedes aegypti* and *Albopictus* mosquitoes, have also increased in Mandor Sub-district. Illegal gold miners are very affected by malaria because of poor hygiene and exhausting work, which lead to poor health; meanwhile, deforestation and still water pools favour mosquito proliferation (Douine et al., 2018).

As a result of these traditional gold mining activities, mercury contamination also occurs in other land uses such as plantations, settlements, and water bodies (Kahha et al., 2019). The soil type that dominates the Mandor Subwatershed itself is ultisol, which is a less fertile soil type. It is highly vulnerable to erosion because it is formed from a clay deposit at the bottom, which decreases water infiltration and increases surface runoff. Ultisol soils have exceptionally low to moderate levels of organic matter, high levels of acidity, few nutrients (N, P, and K), and low CEC (cation exchange capacity) and BS (base saturation) values. This soil can provide its full potential with proper soil management. Infertile soils like ultisol soils are starting to be widely used to support human needs because of inadequate land use practices causing relatively fertile soils to decrease (Karnilawati, 2018). Oil palm plantations and agricultural areas near the mine site may become exposed because of heavy metal contamination from gold mining. Waterlogging and flooding circumstances also make this exposure more severe. So, instead of planting oil palm around the mine, it is recommended to plant tool wood-producing tree vegetation instead.

As well as having a harmful effect on human health, gold mining also contaminates the environment with As, Cr, Ni, Pb, and Zn in addition to mercury (Dan-Badjo et al., 2019). Dan-Badjo et al. (2019) proved the level of contamination in soil, water, and plants of *Datura inoxia* and *Calotropis procera* in Nigeria. Soil contamination was found to reach 555 mg kg^{-1} and 468 mg kg^{-1} for As and Zn, respectively. In water, the highest levels were observed for Zn (540 mg L^{-1}), followed by Cu (7.4 mg L^{-1}) and Al (4.27 mg L^{-1}). The concentrations of As and Zn in the leaves of *Datura inoxia* were 134 mg kg^{-1} and 388 mg kg^{-1}, and in *Calotropis procera* leaves, they were 49 mg kg^{-1} and 46 mg kg^{-1}, respectively.

The findings showed that most of the soil and water samples collected in the gold zone had contamination levels beyond those advised by the WHO, particularly for As, Cr, Ni, Pb, and Zn. The high concentration of As is caused by the runoff and sedimentation of gold mining tailings particles. (Klubi et al., 2018). Moreover, Sousa et al. (2010) found that gold miners in the Amazon River reduced mercury contamination but increased cyanide contamination instead. This condition happened because of modifications made to the barrel washing and amalgamation steps in the gold refining process. Each cycle typically recovers 50% of the gold and lasts 20 days (per vat), using approximately 3300 kg NaCN per month. PVC capsules containing carbon-activated material were placed into the cyanide solution to undertake concentrate leaching. The cycle takes less than 24 hours and recovers up to 98% of the gold in the concentrate. The main advantages of the widespread adoption of this method, apart from the reduced gold recovery cycle and improved recovery, include the possibility of phasing out amalgamation altogether and a marked reduction in cyanide consumption (from the current 22,000 kg to 980 kg per year).

The interconnectedness of mining, social inequalities, and weak environmental management strategies has negatively impacted food sovereignty, especially for local and indigenous communities with low coping capacities (Blanco et al., 2022). Thus, some efforts to overcome and mitigate the negative impacts of traditional gold mining are needed. First, monitoring and treatment programs for land and waters polluted by gold mining are regularly needed to safeguard human health (Dan-Badjo et al., 2019). Second, rigorous integrated impact assessment and conservation planning are needed in mining landscapes to prevent the development of settlements and secondary industries around mining sites while balancing the natural resource-based mining sector's output, livelihoods, and conservation agendas (Seki et al., 2022). Third, plant fast-growing tree vegetation in open areas and around areas contaminated by mining. Fourth, social engineering approaches with conventions will only be successful in reducing ASGM mercury emissions and releases with a comprehensive bottom-up formalized approach among miners, accompanied by significant external funding from consumers, large mining companies, and governments. The estimated 5-year global cost of this approach could be around US$ 213-742 million when scaled per miner or US$ 248-2.17 billion scaled per country (Prescott et al., 2022).

Conclusion

The pattern of changes in vegetation density indicates changing vegetation composition at the study site, which gives a different response to the near-infrared channel and the red channel in the image recording data. The accuracy test value of image classification in the analysis of land use change in 2002 and 2013 amounted to 80%, and in 2022 it amounted to 92%. The process of land degradation in the Mandor Subwatershed within 20 years because of traditional gold mining was indicated by the conversion of forest classes into oil palm plantations and mining lands. A forest area of 11,180.52 hectares in 2002 became 2,953.71 hectares in 2022. This change in forest area shows the increasingly degraded condition of the forest in the Mandor Subwatershed and theoretically might have contributed to the greenhouse gas effect too. Land use change from forested areas to oil palm plantations will certainly have an impact on the exposure of oil palm plantations, especially the production of palm oil in the form of methyl mercury contamination. Moreover, traditional gold mining is a significant global source of mercury (Hg) pollution that not only harms the environment, especially water and soil, but also humans through bioaccumulation and direct exposure. Regular assessment and monitoring of gold mining activities, the right type of vegetation planting, and social engineering approaches can be used to mitigate the impact of pollution due to gold mining activities in the Mandor Subwatershed.

Acknowledgements

The author would like to thank the Faculty of Engineering, Tanjungpura University, for funding this research through DIPA Universitas Tanjungpura Fiscal Year 2022, No. 4566/UN22.4/KU/2022, dated Juni 14, 2022 and Syarifah Apriyanti Nur Hazizah who provided feedback and suggestions as well as discussion on the refinement of this manuscript.

References

Alcaraz-Segura, D., Cabello, J., Paruelo, J.M. and Delibes, M. 2009. Use of descriptors of ecosystem functioning for monitoring a national park network: a remote sensing approach. *Environmental Management* 43(1):38-48, doi:10.1007/s00267-008-9154-y.

Andana, E.K. 2015. Development of Landsat-8 satellite image data for mapping horticultural crop areas with various vegetation index algorithm methods (case study: Malang Regency and its surroundings). *Proceedings of the National Seminar on Technology Management* XXII. Vol. 15 (*in Indonesian*).

Blanco, G.D., Fernández-Llamazares, Á., Blanco, G.D., Baker, J., Tagliari, M.S.M., Hayata, M.A., Campos, M.L. and Hanazaki, N. 2022. The impacts of mining on the food sovereignty and security of indigenous peoples and local communities: a global review. *Science of the Total Environment* 855:158803, doi:10.1016/j.scitotenv.2022.158803.

Cahyono, B.E., Frahma, Y.F. and Nugroho, A.T. 2019. The rate of land cover change using Landsat data in a coal mining area of Sawah Lunto City, Indonesia. *Jurnal Penelitian Fisika dan Aplikasinya* 9(2):189-203, doi:10.26740/jpfa.v9n2.p189-203 (*in Indonesian*).

Carvalho, F.M.V.D., Ferreira, L G., Lobo, F.C., Diniz-Filho, J.A.F. and Bini, L.M. 2008. Padrões de autocorrelação espacial de índices de vegetação MODIS no bioma cerrado. *Revista Árvore* 32:279-290, doi:10.1590/S0100-67622008000200011.

Dan-Badjo, A.T., Ibrahim, O.Z., Guéro, Y., Morel, J.L., Feidt, C. and Echevarria, G. 2019. Impacts of artisanal gold mining on soil, water and plant contamination by trace elements at Komabangou, Western Niger. *Journal of Geochemical Exploration* 205:106328, doi:10.1016/j.gexplo.2019.06.010.

Dero, K., Shiferaw, W. and Zewde, B. 2021. Urban induced land use land cover changes in upper Deme watershed, Southwest Ethiopia. *Journal of Degraded and Mining Lands Management* 9(1):3045-3153, doi:10.15243/jdmlm.2021.091.3045.

Douine, M., Lazrek, Y., Blanchet, D., Pelleau, S., Chanlin, R., Corlin, F., Hureau, L., Volney, B., Hiwat, H., Vreden, S. and Djossou, F. 2018. Predictors of antimalarial self-medication in illegal gold miners in French Guiana: a pathway towards artemisinin resistance. *Journal of Antimicrobial Chemotherapy* 73(1):231-239, doi:10.1093/jac/dkx343.

Hidayat, W., Rustiadi, E. and Kartodihardjo, H. 2015. Impact of mining on land use change and suitability of spatial designation (Case study of East Luwu District, South Sulawesi Province). *Jurnal Perencanaan Wilayah dan Kota* 26(2):130-146, doi:10.5614/jpwk.2015.26.2.5 (*in Indonesian*).

Husodo, T., Ali, Y., Mardiyah, S.R., Shanida, S.S., Abdoellah, O.S. and Wulandari, I. 2021. Satellite image-based vegetation land change in the Citarum watershed, Bandung, West Java. *Majalah Geografi Indonesia* 35(1):54-63, doi:10.22146/mgi.61217 (*in Indonesian*).

Iskandar, M., Sanjoto, T.B. and Sutardji, S. 2012. Vegetation density analysis using remote sensing techniques as a basis for evaluating forest damage in Gunung Gede Pangrango National Park. *Geo-Image* 1(1), doi:10.15294/geoimage.v1i1.953. (*in Indonesian*).

Islam, K., Jashimuddin, M., Nath, B. and Nath, T.K. 2018. Land use classification and change detection by using multi-temporal remotely sensed imagery: The case of Chunati wildlife sanctuary, Bangladesh. *The Egyptian Journal of Remote Sensing and Space Science* 21(1):37-47, doi:10.1016/j.ejrs.2016.12.005.

Islam, K., Vilaysouk, X. and Murakami, S. 2020. Integrating remote sensing and life cycle assessment to quantify the environmental impacts of copper-silver-gold mining: A case study from Laos. *Resources, Conservation and Recycling* 154:104630, doi:10.1016/j.resconrec.2019.104630.

Kahhat, R., Parodi, E., Larrea-Gallegos, G., Mesta, C. and Vázquez-Rowe, I. 2019. Environmental impacts of the life cycle of alluvial gold mining in the Peruvian Amazon rainforest. *Science of the Total Environment* 662:940-951, doi:10.1016/j.scitotenv.2019.01.246.

Karnilawati, K. 2018. Characterization and classification of Ultisol soils in Indrajaya District, Pidie Regency. *Jurnal Ilmiah Pertanian* 14(2):52-59, doi:10.31849/jip.v14i2.437 (*in Indonesian*).

Klubi, E., Abril, J.M., Nyarko, E. and Delgado, A. 2018. Impact of gold-mining activity on trace elements

enrichment in the West African estuaries: The case of Pra and Ankobra rivers with the Volta estuary (Ghana) as the reference. *Journal of Geochemical Exploration* 190:229-244, doi:10.1016/j.gexplo.2018.03.014.

Lambin, E.F., Geist, H.J. and Lepers, E. 2003. Dynamics of land-use and land-cover change in tropical regions. *Annual Review of Environment and Resources* 28(1):205-241, doi:10.1146/annurev.energy.28.050302.105459.

Liu, R.P., Xu, Y.N., Rui, H.C., El-Wardany, R.M. and Dong, Y. 2021. Migration and speciation transformation mechanisms of mercury in undercurrent zones of the Tongguan gold mining area, Shaanxi Loess Plateau and impact on the environment. *China Geology* 4(2):311-328, doi:10.31035/cg2021030.

Mailendra, M. and Buchori, I. 2019. Land damage due to unlicensed gold mining activities around the Singingi River, Kuantan Singingi District. *Jurnal Pembangunan Wilayah dan Kota* 15(3):174-188, doi:10.14710/pwk.v15i3.21304 (*in Indonesian*).

Mason, R.P., Baumann, Z., Hansen, G., Yao, K.M., Coulibaly, M. and Coulibaly, S. 2019. An assessment of the impact of artisanal and commercial gold mining on mercury and methylmercury levels in the environment and fish in Cote d'Ivoire. *Science of the Total Environment* 665:1158-1167, doi:10.1016/j.scitotenv.2019.01.393.

Nugroho, F.S. 2015. Effect of the number of spectral channels, the correlation between spectral channels and the number of object classes on the accuracy of land cover classification. *Jurnal Ilmiah Geomatika* 21(1): 163-170 (*in Indonesian*).

Pang, Q., Gu, J., Wang, H. and Zhang, Y. 2022. Global health impact of atmospheric mercury emissions from artisanal and small-scale gold mining. *Iscience* 25(9):104881, doi:10.1016/j.isci.2022.104881.

Petit, C., Scudder, T. and Lambin, E. 2001. Quantifying processes of land-cover change by remote sensing: resettlement and rapid land-cover changes in south-eastern Zambia. *International Journal of Remote Sensing* 22(17):3435-3456, doi:10.1080/01431160010006881.

Pettorelli, N., Vik, J.O., Mysterud, A., Gaillard, J., Tucker, C.J. and Stenseth, C. 2005. Using the satellite-derived NDVI to assess ecological responses to environmental change. *Trends in Ecology & Evolution* 20(9):503-510, doi:10.1016/j.tree.2005.05.011.

Prescott, G.W., Baird, M., Geenen, S., Nkuba, B., Phelps, J. and Webb, E.L. 2022. Formalizing artisanal and small-scale gold mining: A grand challenge of the Minamata Convention. *One Earth* 5(3):242-251, doi:10.1016/j.oneear.2022.02.005.

Prince, S.D., Becker-Reshef, I. and Rishmawi, K. 2009. Detection and mapping of long-term land degradation using local net production scaling: application to Zimbabwe. *Remote Sensing of Environment* 113(5):1046-1057, doi:10.1016/j.rse.2009.01.016.

Romiyanto, R., Barus, B. and Sudadi, U. 2015. A spatial model of land damage and water pollution due to unlicensed gold mining activities in the Raya river basin, West Kalimantan. *Jurnal Tanah dan Lingkungan* 17(2):47-53, doi:10.29244/jitl.17.2.47-53 (*in Indonesian*).

Rwanga, S.S. and Ndambuki, J.M. 2017. Accuracy assessment of land use/land cover classification using remote sensing and GIS. *International Journal of Geosciences* 8(04):611, doi:10.4236/ijg.2017.84033.

Seki, H.A., Thorn, J.P., Platts, P.J., Shirima, D.D., Marchant, R.A., Abeid, Y., Baker, N., Annandale, M. and Marshall, A.R. 2022. Indirect impacts of commercial gold mining on adjacent ecosystems. *Biological Conservation* 275:109782, doi:10.1016/j.biocon.2022.109782.

Siahaya, W.A., Danoedoro, P., Khakhim, N. and Baiquni, M. 2015. The comparison analysis of land cover change based on vegetation index and multispectral classification (Case study Leihitu Peninsula Ambon City District). *Journal of Degraded and Mining Lands Management* 2(4):415-426, doi:10.15243/jdmlm.2015.024.415.

Son, N.T., Chen, C.F., Chen, C.R., Minh, V.Q. and Trung, N.H. 2014. A comparative analysis of multitemporal MODIS EVI and NDVI data for large-scale rice yield estimation. *Agricultural and Forest Meteorology* 197:52-64, doi:10.1016/j.agrformet.2014.06.007.

Sousa, R.N., Veiga, M.M., Klein, B., Telmer, K., Gunson, A.J. and Bernaudat, L. 2010. Strategies for reducing the environmental impact of reprocessing mercury-contaminated tailings in the artisanal and small-scale gold mining sector: insights from Tapajos River Basin, Brazil. *Journal of Cleaner Production* 18(16-17):1757-1766, doi:10.1016/j.jclepro.2010.06.016.

Sudiana, D. and Diasmara, E. 2008. Vegetation Index Analysis using NOAA/AVHRR and TERRA/AQUA-MODIS Satelit Satellite Data. *Seminar on Intelligent Technology and Its Applications* 3(2):423-428. (*in Indonesian*).

Triana, L., Nurjazuli, N. and Wahyuningsih, N.E. 2013. Analysis of mercury heavy metal contamination in water and shrimp in Mandor river, Mandor sub-district, Landak district. *Jurnal Kesehatan Lingkungan Indonesia* 11(2):144-152 (*in Indonesian*).

Ulrich, S., Trench, A. and Hagemann, S. 2022. Gold mining greenhouse gas emissions, abatement measures, and the impact of a carbon price. *Journal of Cleaner Production* 340:130851, doi:10.1016/j.jclepro.2022.130851.

USGS. 2016, Landsat-Earth Observation Satellites, Fact Sheet 2015-3081, ver. 1.1, U.S. Department of the Interior, U.S. Geological Survey.

Wang, Q., Adiku, S., Tenhunen, J. and Granier, A. 2005. On the relationship of NDVI with leaf area index in a deciduous forest site. *Remote Sensing of Environment* 94(2):244-255, doi:10.1016/j.rse.2004.10.006.

Yengoh, G.T., Dent, D., Olsson, L., Tengberg, A.E. and Tucker III, C.J. 2015. Use of the Normalized Difference Vegetation Index (NDVI) to assess Land degradation at multiple scales: current status, future trends, and practical considerations. Lund University Center for Sustainability Studies (LUCSUS), and The Scientific and Technical Advisory Panel of the Global Environment Facility (STAP/GEF), doi:10.1007/978-3-319-24112-8.

Yudistira, R., Meha, A.I. and Prasetyo, S.Y.J. 2019. Land conversion changes using NDVI, EVI, SAVI and PCA on Landsat 8 Imagery (Case Study: Salatiga City). *Indonesian Journal of Computing and Modeling* 2(1):25-30 (*in Indonesian*).